Electronic Supplementary Material (ESI) for Journal of Materials Chemistry B.

Electronic Supplementary Information

Fabrication of Au Aerogels with {110}-Rich Facets by Size-dependent Surface Reconstruction for Enzyme-free Glucose Detection

Cui Wang,[a] Wenchao Duan,[a] Lixiang Xing,[a] Yujiao Xiahou,[a] Wei Du,[b] and Haibing Xia*, [a]

[a] State Key Laboratory of Crystal Materials, Shandong University, Jinan, 250100, P. R. China.
[b] School of Environment and Material Engineering, Yantai University, Yantai 264005, Shandong, China.
*E-mail: hbxia@sdu.edu.cn

Scheme S1 Schematic representation of formation process of Au[6-16] aerogels at the optimal particle ratio. R is the size ratio of large Au NPs (16 nm) to small Au NPs (6 nm). No surface construction occurs at this R. {111} and {100} facets were labelled and black lines on the surface of 16 nm Au NPs represent {110} facets.

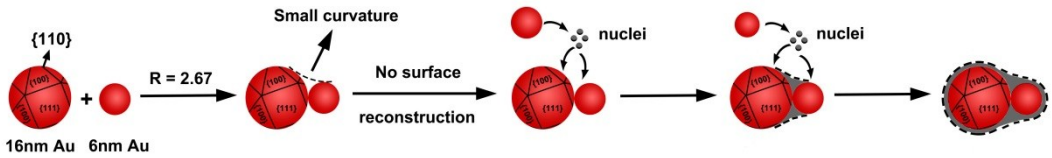

Scheme S2 Schematic representation of formation process of Au[6-30] aerogels at the optimal particle ratio. R is the size ratio of large Au NPs (30 nm) to small Au NPs (6 nm). Surface reconstruction slightly occurs at the critical R. {111} and {100} facets were labelled and black lines on the surface of 30 nm Au NPs represent {110} facets.

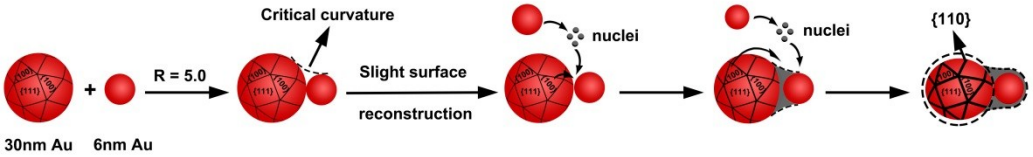

Scheme S3 Schematic representation of formation process of Au[6-50] aerogels at the particle ratio of bigger than the optimal ratio. R is the size ratio of large Au NPs (50 nm) to small Au NPs (6 nm). Surface reconstruction obviously occurs at the R. However, the {110} facets would disappear and transfer into {100} facets due to the further overgrowth. {111} and {100} facets were labelled and black lines on the surface of 50 nm Au NPs represent {110} facets.

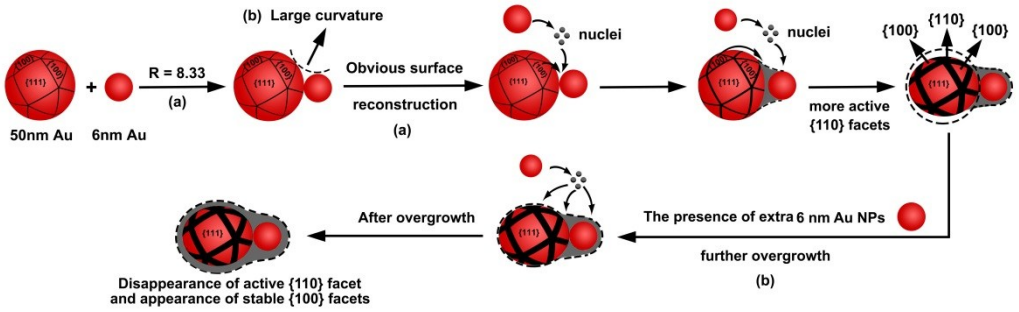

Fig. S1 TEM images of 6 nm Au NPs (a), 16 nm Au NPs (b), 30 nm Au NPs (c), and 50 nm Au NPs (d).

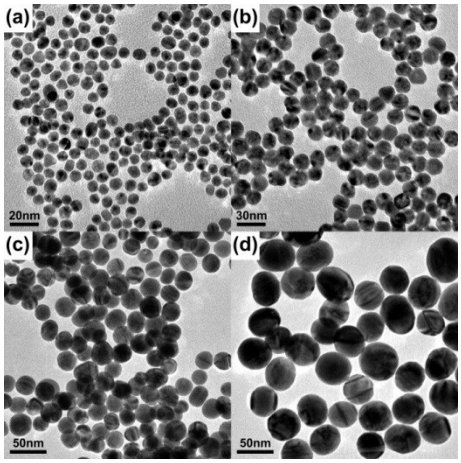

Fig. S2 CV curves of $Au^{6\text{-}16}$ aerogels (A), $Au^{6\text{-}30}$ aerogels (B), and $Au^{6\text{-}50}$ aerogels (C) prepared at the different particle ratios, measured in 0.5 M H_2SO_4 with a scan rate of 50 mV s^{-1} in the region of -0.3 ~ 1.5 V. The particle ratios of 6 nm to 16 nm Au NPs used for synthesis of the corresponding $Au^{6\text{-}16}$ aerogels with different exposed surface facets (Fig. 1A) are (a) 2, (b) 9, and (c) 36, respectively. The particle ratios of 6 nm to 30 nm Au NPs used for synthesis of $Au^{6\text{-}30}$ aerogels with different exposed surface facets (Fig. 1B) are (a) 3, (b) 12, and (c) 48, respectively. The particle ratios of 6 nm to 50 nm Au NPs used for synthesis of $Au^{6\text{-}50}$ aerogels with different exposed surface facets (Fig. 1C) are (a) 8, (b) 24, and (c) 96, respectively. In each case, the particle number of 6 nm Au NPs was fixed.

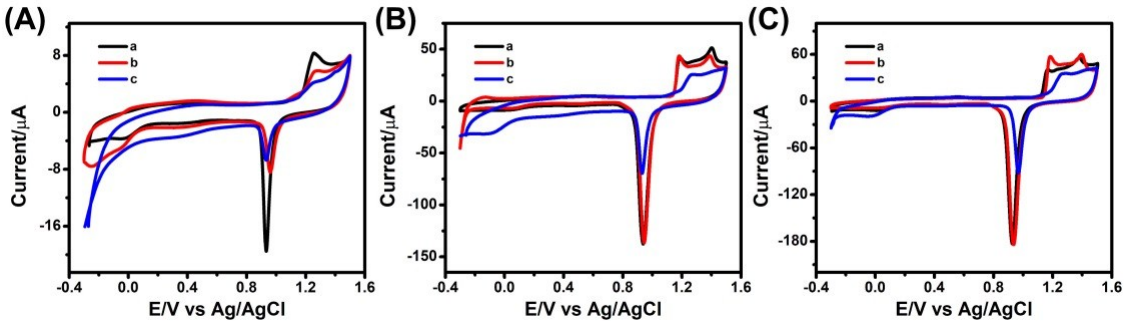

Fig. S3 De-convoluted CV curves of $Au^{6\text{-}23}$ aerogels (a), and $Au^{6\text{-}35}$ aerogels (b), which were measured in H_2SO_4 (0.5 M) with a scan rate of 50 mV s^{-1}.

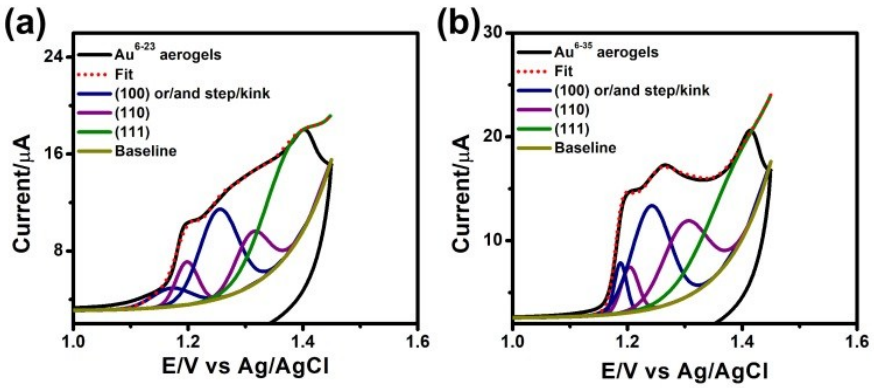

Additionally, the ratio of facets exposed on the surface of $Au^{6\text{-}23}$ aerogels and $Au^{6\text{-}35}$ aerogels were also calculated by de-convoluting their CV curves (Fig. S3, Table S1). The ratio of {110}, {100} and {111} facets in $Au^{6\text{-}23}$ aerogels are calculated to be 18.72%, 35.73%, and 45.55%, respectively. Moreover, the ratio of {110}, {100} and {111} facets in $Au^{6\text{-}35}$ aerogels are calculated to be 26.86%, 29.66%, and 43.48%, respectively. It is clear that the ratio of {110} in $Au^{6\text{-}23}$ aerogels is a little lower than those in 6 nm Au NPs and $Au^{6\text{-}30}$ aerogels (Table 1). In addition, the ratio of {110} facets in $Au^{6\text{-}35}$ aerogels is relatively higher than that of 6 nm Au NPs and $Au^{6\text{-}30}$ aerogels.

Fig. S4 De-convoluted CV curves of 6 nm Au NPs (a), 16 nm Au NPs (b), 30 nm Au NPs (c), and 50 nm Au NPs (d), which were measured in H_2SO_4 (0.5 M) with a scan rate of 50 mV s^{-1}.

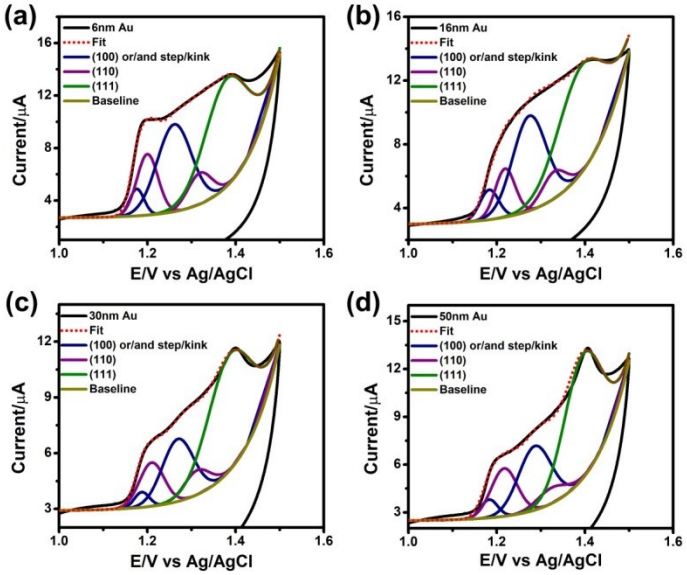

Fig. S5 TEM images of the corresponding intermediates taken out at different times after the addition of NaCl solution into the mixed aqueous dispersions of Au NPs of 6 and 16 nm at the optimal particle ratio: (a) 0 min, (b) 1 min, (c) 5 min, (d) 12 min, (e) 30 min, (f) 1 h, (g) 3 h, and (h) 6 h. The insets in (a-h) are photographs of corresponding color of mixed aqueous dispersions of Au NPs in the presence of NaCl at different times.

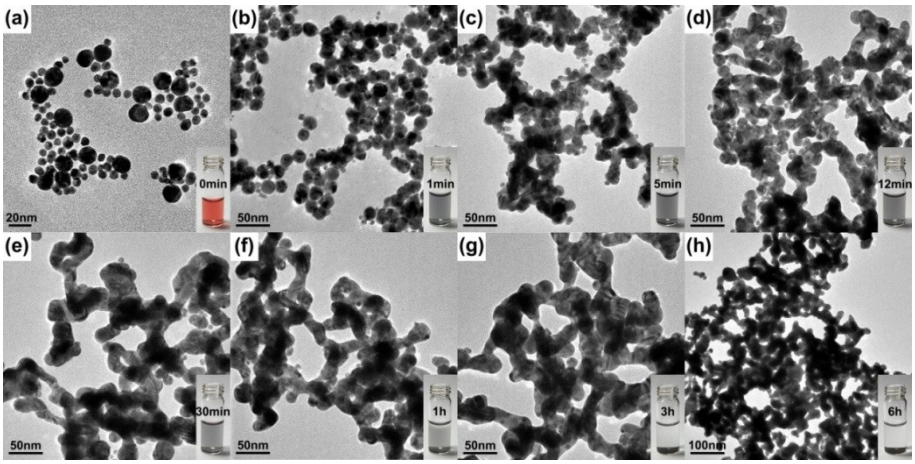

Fig. S6 TEM images of the corresponding intermediates taken out at different times after the addition of NaCl solution into the mixed aqueous dispersions of Au NPs of 6 and 30 nm at the optimal particle ratio: (a) 0 min, (b) 1 min, (c) 3 min, (d) 5 min, (e) 10 min, (f) 30 min, (g) 1 h, and (h) 4 h. The insets in (a-h) are photographs of corresponding color of mixed aqueous dispersions of Au NPs in the presence of NaCl at different times.

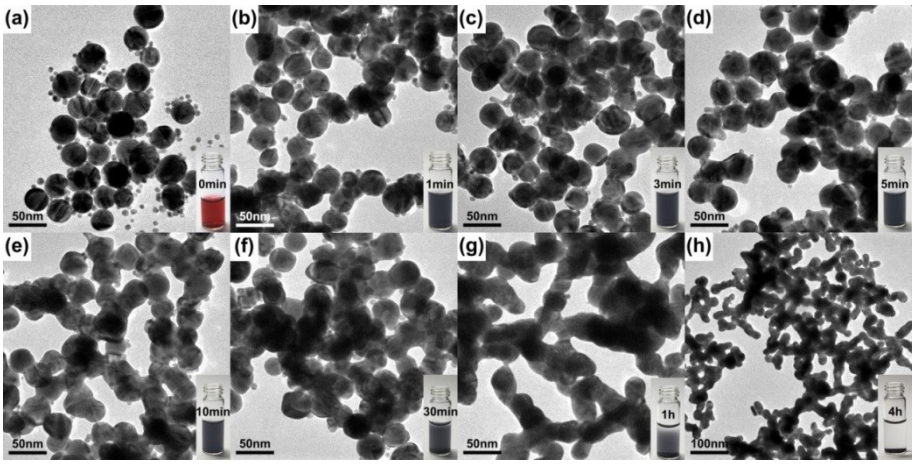

Fig. S7 TEM images of the corresponding intermediates taken out at different times after the addition of NaCl solution into the mixed aqueous dispersions of Au NPs of 6 and 50 nm at the optimal particle ratio: (a) 0 min, (b) 1 min, (c) 3 min, (d) 5 min, (e) 10 min, (f) 30 min, (g) 1 h, and (h) 3 h. The insets in (a-h) are photographs of corresponding color of mixed aqueous dispersions of Au NPs in the presence of NaCl at different times.

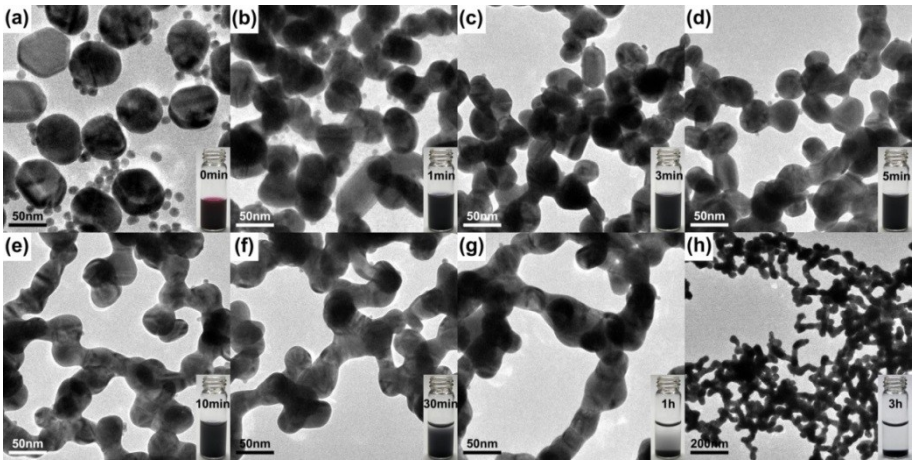

Fig. S8 High magnification TEM images of $Au^{6\text{-}16}$ aerogels (a, b, and c), $Au^{6\text{-}30}$ aerogels (d, e, and f), and $Au^{6\text{-}50}$ aerogels (g, h, and i) containing the maximum ratio of {110}-facets on the surfaces, respectively. The atom steps were labelled by red ({100} (0.204 nm) or {110} (0.144nm) facets) and black ({111} facets (0.235 nm)) short lines, respectively.

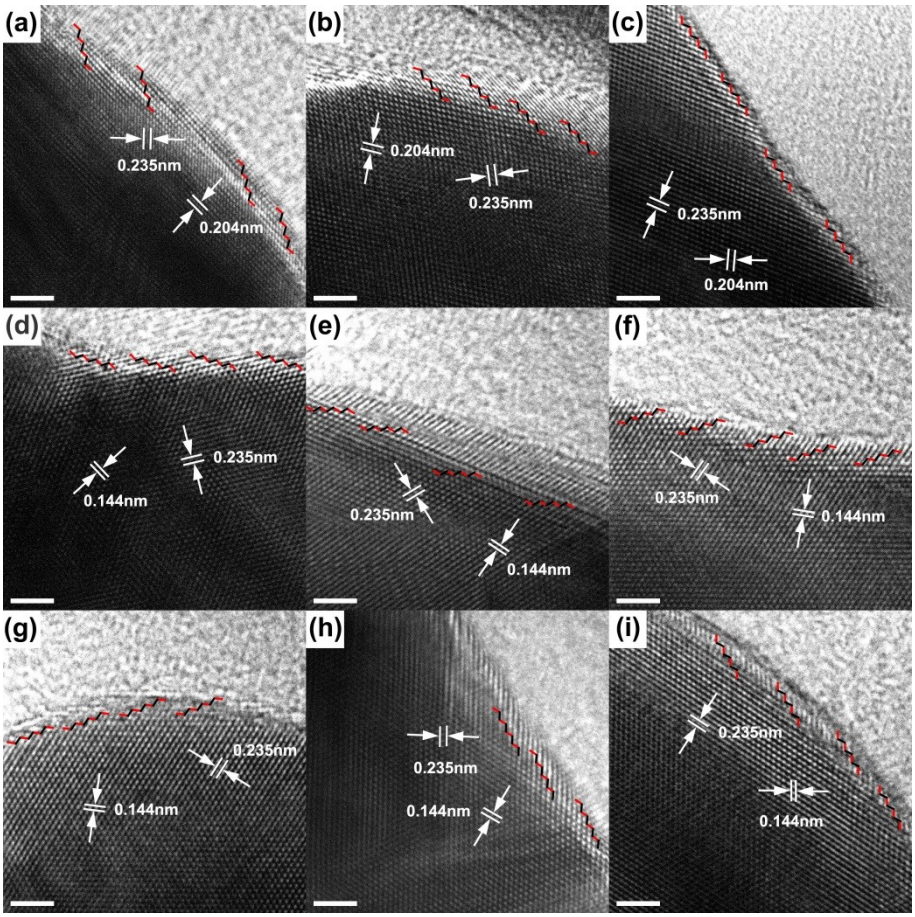

Fig. S9 Comparison of the calculated ratios of the response current of glucose-to-AA and glucose-to-UA on Au[6-50] aerogels with the highest ratio of {110}-facets at seven different applied potentials. The concentration of glucose, AA, and UA are 0.5 mM, 0.05 mM and 0.05 mM, respectively.

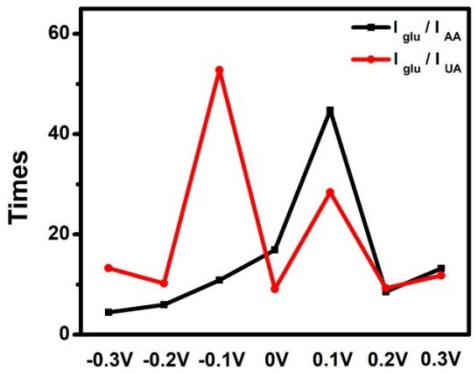

Fig. S10 CV curves of the corresponding Au^{m-n} aerogels with the highest ratio of {110}-facets in NaOH (0.1 M): Au^{6-16} aerogels (black), Au^{6-30} aerogels (red) and Au^{6-50} aerogels (blue). Scan rate: 50 mV s^{-1}.

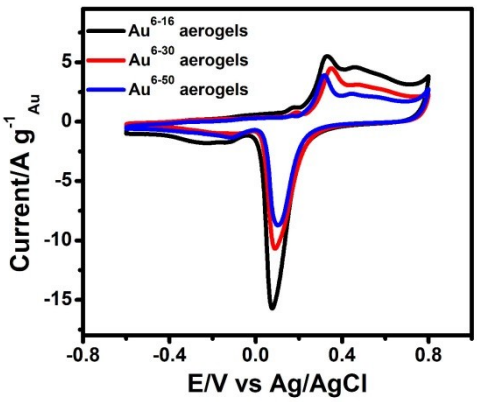

Fig. S11 (a) Amperometric responses of different concentrations of glucose on Au[6-16] aerogels with the highest ratio of {110}-facets at the optimal applied potential of 0.1 V. The glucose was successively added into the NaOH solution (0.1 M) under a continuous stirring condition. (b) The corresponding calibration curve obtained by plotting the response currents of each concentration of glucose at the steady state. The insets in (a) and (b) are the local enlargements of the areas labeled by dashed red line.

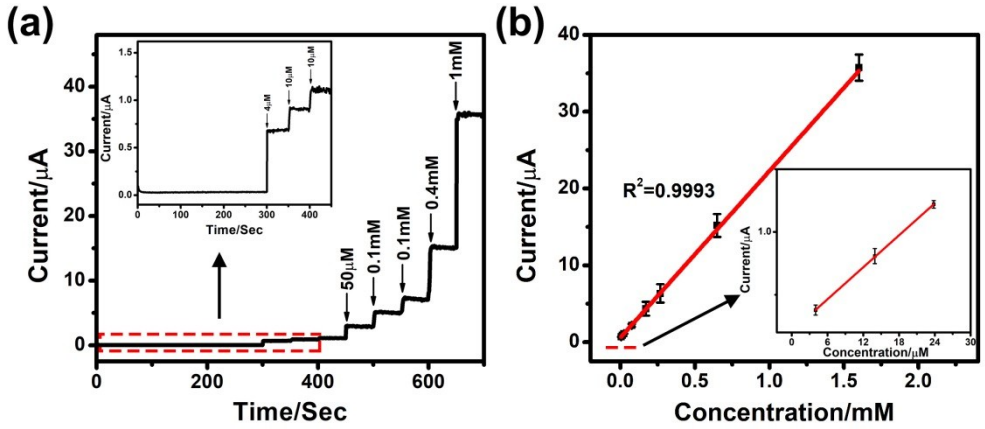

Fig. S12 (a) Amperometric responses of different concentrations of glucose on Au[6-30] aerogels with the highest ratio of {110}-facets at the optimal applied potential of 0.1 V. The glucose was successively added into the NaOH solution (0.1 M) under a continuous stirring condition. (b) The corresponding calibration curve obtained by plotting the response currents of each concentration of glucose at the steady state. The insets in (a) and (b) are the local enlargements of the areas labeled by dashed red line.

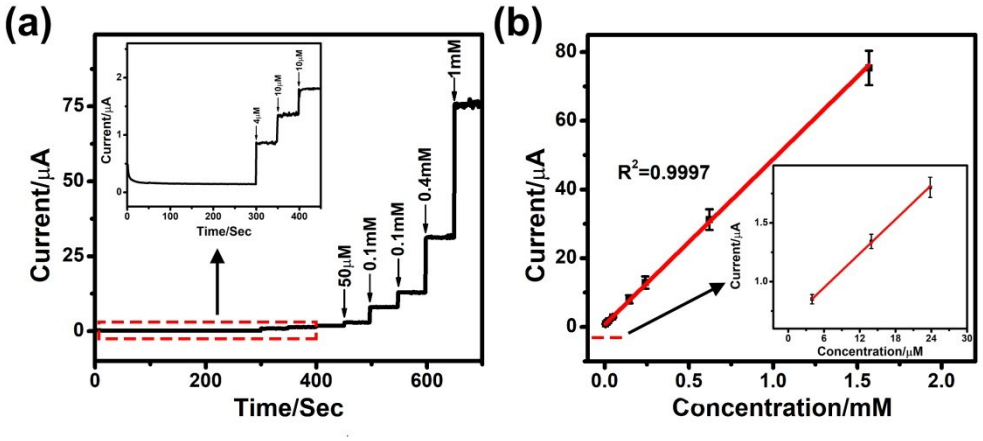

Fig. S13 (a) Amperometric responses of glucose (0.2 mM) on GCEs modified by a batch of three Au$^{6\text{-}50}$ aerogels with the highest ratio of {110}-facets at the optimal applied potential of 0.1 V. The glucose was successively added into the NaOH (0.1 M) under a continuous stirring condition. (b) The corresponding calibration curve obtained by plotting the response currents of each concentration of glucose at the steady state.

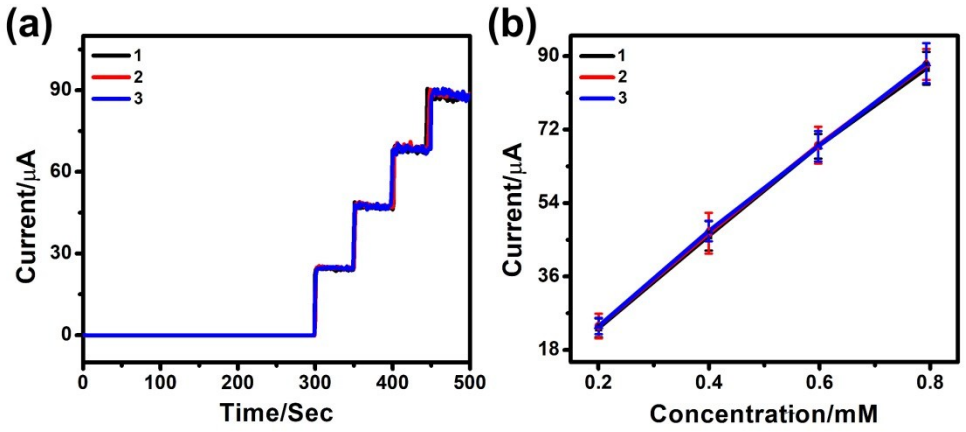

Fig. S14 (a) CV curves and (b) corresponding line charts selected from the successive potential cycling of $Au^{6\text{-}50}$ aerogels with the highest ratio of {110}-facets in NaOH (0.1 M) containing glucose (5 mM). Scan rate: 50 mV s^{-1}. (c) Histogram of the amperometric responses of glucose (5 mM) on $Au^{6\text{-}50}$ aerogels with the highest ratio of {110}-facets in NaOH (0.1 M) under a continuous stirring condition at the optimal applied potential of 0.1 V within 5 weeks storage period. The amperometric response in the first week is defined as 100%. Error bars represent the standard deviations among three measurements.

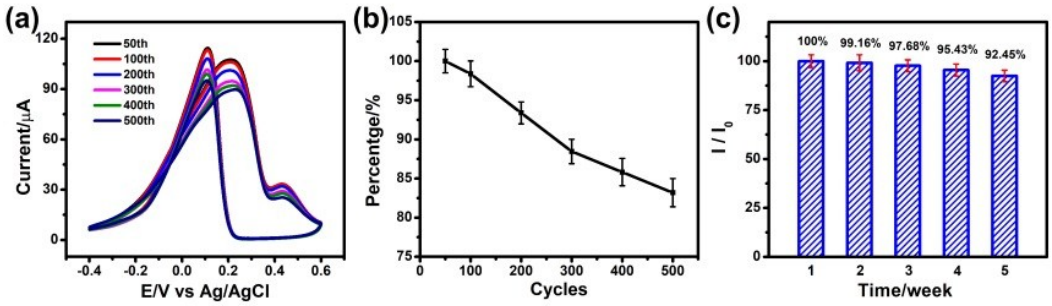

Table S1 Detailed recipes for synthesis of selected three groups of Au^{m-n} aerogels.

Au^{m-n} aerogels	Particle ratio of 6nm Au to 16, 23, 30, 35, or 50nm Au	Volume of 6nm Au solution (mL)	Particle ratio of 6nm Au (NPs/mL)	Volume of 16, 23, 30, 35 or 50nm Au solution (mL)	Particle ratio of 16, 23, 30, 35, or 50nm Au solution (NPs/mL)
Au^{6-16}	6nm:16nm=1:1/2	0.74	$1.76*10^{13}$	1.26	$5.18*10^{12}$
Au^{6-16}	6nm:16nm=1:1/9	0.74	$1.76*10^{13}$	1.26	$1.15*10^{12}$
Au^{6-16}	6nm:16nm=1:1/36	0.74	$1.76*10^{13}$	1.26	$2.87*10^{11}$
Au^{6-23}	6nm:23nm=1:1/10	0.74	$1.76*10^{13}$	1.26	$1.76*10^{12}$
Au^{6-30}	6nm:30nm=1:1/3	0.74	$1.76*10^{13}$	1.26	$3.45*10^{12}$
Au^{6-30}	6nm:30nm=1:1/12	0.74	$1.76*10^{13}$	1.26	$8.61*10^{11}$
Au^{6-30}	6nm:30nm=1:1/48	0.74	$1.76*10^{13}$	1.26	$2.15*10^{11}$
Au^{6-35}	6nm:16nm=1:1/12	0.74	$1.76*10^{13}$	1.26	$8.61*10^{11}$
Au^{6-50}	6nm:50nm=1:1/8	0.74	$1.76*10^{13}$	1.26	$1.29*10^{12}$
Au^{6-50}	6nm:50nm=1:1/24	0.74	$1.76*10^{13}$	1.26	$4.31*10^{11}$
Au^{6-50}	6nm:50nm=1:1/96	0.74	$1.76*10^{13}$	1.26	$1.08*10^{11}$

Note that the particle number of 6 nm Au NPs was fixed and that of other Au NPs (16, 23, 30, 35, and 50 nm) was accordingly adjusted. In addition, the volume of other Au NPs (16, 23, 30, 35 and 50 nm) was diluted or concentrated to 1.26 mL for further use but keeping their corresponding particle number. In addition, the particle ratios used for synthesis of Au^{6-23} and Au^{6-35} aerogels are the optimal.

Table S2 Comparison of average sizes of thin and thick ligaments, and islands in the $Au^{6\text{-}16}$ aerogels, $Au^{6\text{-}30}$ aerogels, and $Au^{6\text{-}50}$ aerogels, which all obtained at the optimal particle ratios.

Sample	averages size of thin ligaments (nm)	averages size of thick ligaments (nm)	averages size of islands(nm)
$Au^{6\text{-}16}$ aerogels	11.2±1.5	25.3±3.6	62.3±6.5
$Au^{6\text{-}30}$ aerogels	20.6±3.1	38.2±4.5	89.9±8.0
$Au^{6\text{-}50}$ aerogels	33.2±4.5	52.0±5.4	102±9.5

Table S3 Comparison of the response time of our sample in glucose detection with that reported in literatures.

Electrode materials	Medium	Response time	Ref
$Au^{6\text{-}50}$ aerogels	0.1 M NaOH	2s	This work
HNPG/AuSn	0.1 M NaOH	4s	[1]
Porous gold cluster	0.2 M NaOH	5s	[2]
Co-MOF nanosheet	0.1 M NaOH	3s	[3]
Au NPs modified CuO NWs	0.1 M NaOH	5s	[4]

HNPG represents highly nanoporous gold film, NWs represents nanowires.

References

1 Y. Pei, M. Hu, F. Tu, X. Tang, W. Huang, S. Chen, Z. Li and Y. Xia, *Biosens. Bioelectron.*, 2018, **117**, 758– 765.

2 L. Han, S. Zhang, L. Han, D.-P. Yang, C. Hou and A. Liu, *Electrochimica Acta*, 2014, **138**, 109–114.

3 Y. Li, M. Xie, X. Zhang, Q. Liu, D. Lin, C. Xu, F. Xie and X. Sun, *Sens. Actuators B*, 2019, **278**, 126-132.

4 A. K. Mishra, B. Mukherjee, A. Kumar, D. K. Jarwal, S. Ratan, C. Kumar and S. Jit, *RSC Adv.*, 2019, **9**, 1772-1781.